ACKNOWLEDGMENTS

We thank M. Sawaya and M. Collazo for their assistance with crystallography, conducted at the UCLA-DOE X-ray Crystallization and Crystallography Core Facilities, which are supported by DOE grant DE-FC02-02ER63421. We thank M. Capel, K. Rajashankar, N. Sukumar, J. Schuermann, I. Kourinov, and F. Murphy at Northeastern Collaborative Access Team beamlines 24-ID-E and 24-ID-C at the Advanced Photon Source (APS), which are supported by grants from the National Center for Research Resources (5P41RR015301-10) and the National Institute of General Medical Sciences (8 P41 GM103403-10) of the National Institutes of Health. Use of the APS is supported by DOE under contract no. DE-AC02-06CH11357. We thank the staff at the Advanced Light Source SIBYLS beamline at Lawrence Berkeley National Laboratory, including K. Burnett, G. Hura, M. Hammel, J. Tanamachi, and J. Tainer for the services provided through the mail-in SAXS program, which is supported by the DOE Office of Biological and Environmental Research Integrated Diffraction Analysis program and the NIH project MINOS (Macromolecular Insights on Nucleic Acids Optimized by Scattering; grant no. RO1GM105404). We also thank U. Nattermann for help with EM, Y. Hsia for assistance with light-scattering experiments, C. Stafford for mass spectroscopy assistance, B. Nickerson for assistance with in vitro assembly experiments, and G. Rocklin for providing scripts used in data analysis. This work was supported by the Howard Hughes Medical Institute (S.G., D.C., T.G., and D.B.) and its Janelia Research Campus visitor program (S.G.), the Bill and Melinda Gates Foundation (D.B. and N.P.K.), Takeda Pharmaceutical Company (N.P.K.), NSF (grant no. CHE-1332907 to D.B. and T.O.Y.), the Air Force Office of Scientific Research (grant no. FA950-12-10112 to D.B.), and the Defense Advanced Research Projects Agency (grant no. W911NF-14-1-0162 to D.B. and N.P.K.). Y.L. was supported by a Whitcome Fellowship through the UCLA Molecular Biology Institute, and J.B.B. was supported by a NSF graduate research fellowship (grant no. DGE-0718124). Coordinates and structure factors were deposited in the Protein Data Bank with accession codes 5IM5 (I53-40), 5IM4 (I52-32), and 5IM6 (I32-28). J.B.B., W.S., N.P.K., D.E., and D.B. have filed a nonprovisional U.S. patent application, no. 14/930,792, related to the work presented herein.

SUPPLEMENTARY MATERIALS

www.sciencemag.org/content/353/6297/389/suppl/DC1
Materials and Methods
Supplementary Text
Figs. S1 to S13
Tables S1 to S6
References (*38*–*60*)
Databases S1 to S3

15 April 2016; accepted 21 June 2016
10.1126/science.aaf8818

MITOCHONDRIA

Mitochondrial endonuclease G mediates breakdown of paternal mitochondria upon fertilization

Qinghua Zhou,[1]*† Haimin Li,[1]* Hanzeng Li,[1,2]* Akihisa Nakagawa,[1] Jason L. J. Lin,[3] Eui-Seung Lee,[1] Brian L. Harry,[1,4] Riley Robert Skeen-Gaar,[1] Yuji Suehiro,[5] Donna William,[6] Shohei Mitani,[5] Hanna S. Yuan,[3] Byung-Ho Kang,[7]‡ Ding Xue[1]‡

Mitochondria are inherited maternally in most animals, but the mechanisms of selective paternal mitochondrial elimination (PME) are unknown. While examining fertilization in *Caenorhabditis elegans*, we observed that paternal mitochondria rapidly lose their inner membrane integrity. CPS-6, a mitochondrial endonuclease G, serves as a paternal mitochondrial factor that is critical for PME. We found that CPS-6 relocates from the intermembrane space of paternal mitochondria to the matrix after fertilization to degrade mitochondrial DNA. It acts with maternal autophagy and proteasome machineries to promote PME. Loss of *cps-6* delays breakdown of mitochondrial inner membranes, autophagosome enclosure of paternal mitochondria, and PME. Delayed removal of paternal mitochondria causes increased embryonic lethality, demonstrating that PME is important for normal animal development. Thus, CPS-6 functions as a paternal mitochondrial degradation factor during animal development.

Mitochondria are critical for many cellular processes including cellular respiration, apoptosis, and metabolism, and they possess their own genome (mtDNA) (*1*, *2*). However, only maternal mitochondria are passed on to progeny. Although elimination of paternal mtDNA can occur at various developmental stages through different mechanisms (*3*), it is unclear why and how paternal mitochondria are selectively eliminated after fertilization during embryo development (*3*, *4*). To address these questions, we examined paternal mitochondria in *C. elegans* spermatozoa and embryos by electron microscopy (EM) and tomography.

Mitochondria in wild-type (N2) spermatozoa are spherical (fig. S1A), with an average diameter of 464 ± 68 nm (SD), and their cristae, formed by extensive infolding of the inner membrane, uniformly distribute in the matrix (Fig. 1A). Paternal mitochondria in N2 zygotes are readily distinguished from the tubular and thinner maternal mitochondria (with an average width of 238 ± 57 nm; fig. S1B). Notably, all paternal mitochondria in N2 zygotes have multiple dark aggregates (agg) in the matrix that form promptly after their entry into oocytes (Fig. 1, B and E, fig. S1, B to G, and movie S1). The double-layer membranes from autophagosomes have started to assemble around some paternal mitochondria at this stage (fig. S1B). We named paternal mitochondria containing small aggregates that lack nearby autophagosome membranes "small agg PM" (Fig. 1B). Those containing larger aggregates that are associated with autophagosome membranes are called "large agg PM" (Fig. 1C), and those with few cristae and enclosed in an autophagosome are called "ghost PM" (Fig. 1D). Many small agg PM arise independently of the autophagy machinery (Fig. 1, B and E, fig. S1, B to G, and movie S1). Large agg PM and ghost PM are observed in N2 zygotes but are mostly seen in two- or four-cell–stage embryos (Fig. 1, C to E).

In large agg PM, cristae are cleared from the central region as the aggregates enlarge in the matrix (Fig. 1C), which occurs before autophagosomes enclose paternal mitochondria. Once enclosed by autophagosomes, they lose matrix contents except for some remaining aggregates, but their outer membrane does not rupture until most of the cristae have disappeared (Fig. 1D and fig. S1H). These results suggest that paternal mitochondria are destroyed partly in embryos by self-initiated internal breakdown prior to autophagosome assembly and degradation.

To identify intrinsic mitochondrial factors involved in paternal mitochondrial elimination (PME), we performed an RNA interference (RNAi) screen against 217 *C. elegans* nuclear genes predicted to encode mitochondrial proteins (table S1), using a sensitive polymerase chain reaction (PCR)–based method and a 3053–base pair (bp) mtDNA deletion allele (*uaDf5*; Fig. 2A) to track the fate of mtDNA (*5*). *uaDf5* mtDNA was detected in cross-progeny at all developmental stages from mating of N2 males with *uaDf5/+* heteroplasmic hermaphrodites (fig. S2A) (*5*) but was detected only in early embryos, not in late embryos nor in larval cross-progeny from N2 hermaphrodites mated with *uaDf5/+* males (Fig. 2B); these findings indicate that PME is conserved in *C. elegans* (*5*–*7*). RNAi of the *cps-6* gene, which encodes a homolog of human mitochondrial endonuclease G (*8*, *9*), caused persistence of

[1]Department of Molecular, Cellular, and Developmental Biology, University of Colorado, Boulder, CO 80309, USA. [2]Department of Chemistry and Biochemistry, University of Colorado, Boulder, CO 80309, USA. [3]Institute of Molecular Biology, Academia Sinica, Taipei 11529, Taiwan. [4]Medical Scientist Training Program, University of Colorado, Aurora, CO 80045, USA. [5]Department of Physiology, Tokyo Women's Medical University, School of Medicine and CREST, Japan Science and Technology Agency, Tokyo 162-8666, Japan. [6]Department of Microbiology and Cell Science, University of Florida, Gainesville, FL 32611, USA. [7]School of Life Sciences, Centre for Cell and Developmental Biology and State Key Laboratory of Agrobiotechnology, Chinese University of Hong Kong, Hong Kong, China.
*These authors contributed equally to this work. †Present address: First Affiliated Hospital, Biomedical Translational Research Institute, Jinan University, Guangzhou 510630, China. ‡**Corresponding author. Email: ding.xue@colorado.edu (D.X.); bkang@cuhk.edu.hk (B.-H.K.)**

paternal *uaDf5* mtDNA until the late stages of embryogenesis—a finding not observed in RNAi of other genes (fig. S2B and supplementary materials). A 336-bp deletion *(tm3222)* in *cps-6*, which removes the catalytic site of CPS-6 (fig. S2C) (*10*), had the same effect as *cps-6(RNAi)*, leading to persistence of paternal *uaDf5* mtDNA throughout embryo development (Fig. 2C), whereas *uaDf5* was detected only in 64-cell or earlier embryos in crosses between *uaDf5*/+ males and N2 hermaphrodites (Fig. 2B). These results indicate that *cps-6* is associated with rapid removal of paternal mtDNA during early embryogenesis.

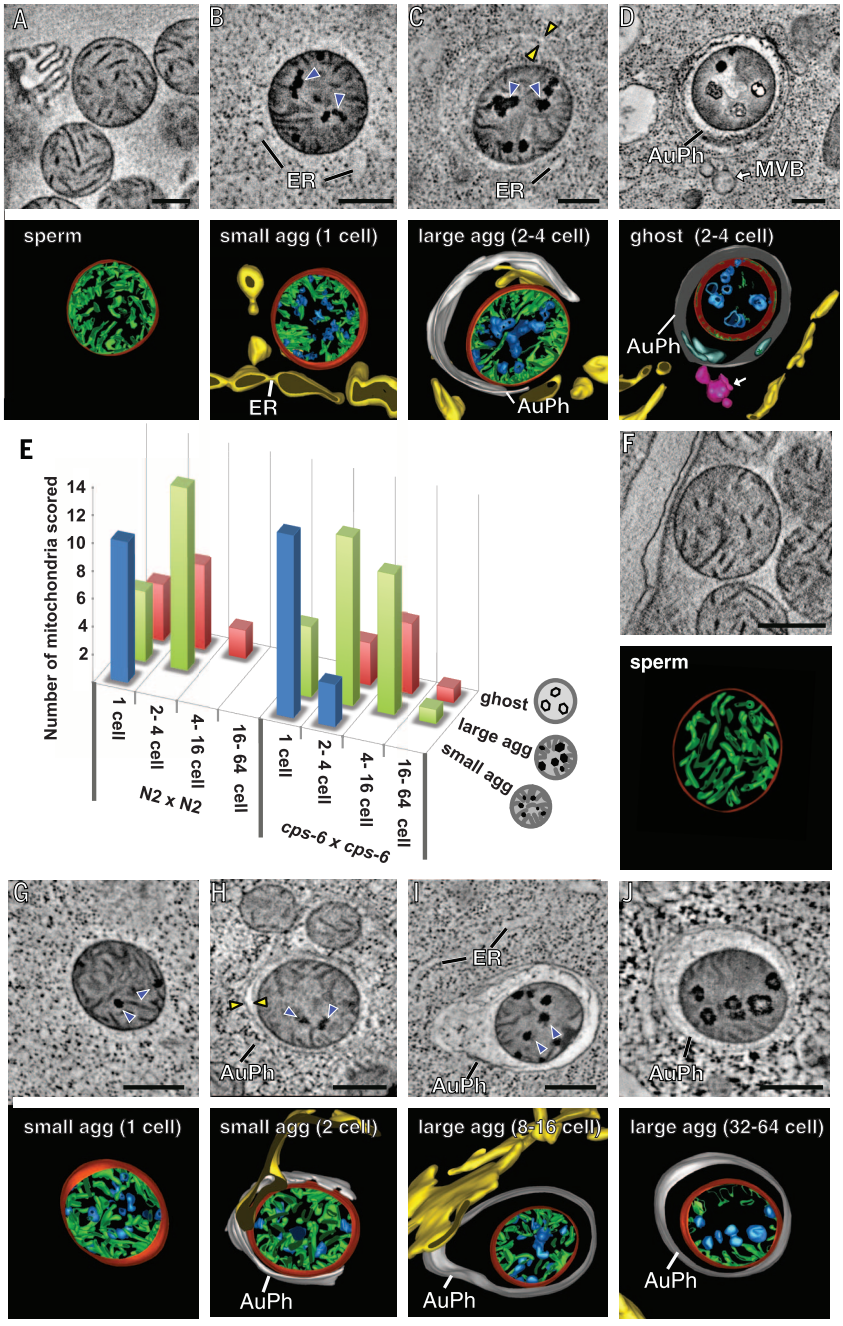

Fig. 1. Loss of *cps-6* delays internal breakdown of paternal mitochondria after fertilization. (**A** to **D**, **F** to **J**) Tomographic slice images and corresponding 3D models of a mitochondrion in an N2 (A) or *cps-6(tm3222)* (F) spermatozoon or a paternal mitochondrion in an N2 embryo [(B) to (D)] or a *cps-6(tm3222)* embryo [(G) to (J)] at the indicated stages. 3D models of autophagosomes (AuPh) and endoplasmic reticulum (ER) are shown. Mitochondrial membranes, cristae, and aggregates are colored red, green, and blue, respectively. Dark aggregates and autophagosome membranes are indicated with blue and yellow arrowheads, respectively. Scale bars, 300 nm. (**E**) Histogram showing three classes of paternal mitochondria in embryos of different stages from the indicated N2 cross (n = 45) or *cps-6(tm3222)* cross (n = 56).

We performed microscopic analysis to monitor the disappearance of paternal mitochondria stained by Mitotracker Red (MTR), a mitochondrion-specific dye (*5*). When MTR-stained N2 males were mated with unstained N2 hermaphrodites, MTR-stained paternal mitochondria were seen in embryos before the 64-cell stage (fig. S3, A to G), indicating that PME occurs in concert with paternal mtDNA elimination (Fig. 2B). Conversely, loss of *cps-6* resulted in persistence of MTR paternal mitochondria to around the 550-cell stage (fig. S3, H to N), confirming that CPS-6 promotes rapid clearance of paternal mitochondria.

CPS-6 was first identified as an apoptotic nuclease that translocates from mitochondria to the nucleus during apoptosis to mediate chromosome fragmentation (*8*, *9*). A nonapoptotic role of CPS-6 in *C. elegans* has not been reported. We used both the PCR assay and the microscopic assay to investigate whether CPS-6 is required paternally or maternally for PME (supplementary text) and found that a significant portion of paternal mitochondria and mtDNA persisted past the 64-cell stage when paternal *cps-6* was defective (Fig. 2, D and E, matings 3 and 4). By contrast, embryos without maternal *cps-6* displayed normal PME (Fig. 2, D and E, mating 2). These results indicate that paternal CPS-6 is required to promote PME.

CPS-6 is imported into mitochondria through a mitochondrial targeting sequence (amino acids 1 to 21), because CPS-6ΔN, lacking this targeting sequence, localizes to the nucleus (*8*). Expression of CPS-6, but not CPS-6ΔN, in *cps-6(tm3222)* males through the ubiquitously expressed *dpy-30* gene promoter rescued the defect in PME (Fig. 2F, matings 1, 2, and 5 to 7; see also supplementary text), indicating that localization of CPS-6 in paternal mitochondria is required to mediate PME. Because expression of the nuclease-deficient CPS-6(H148A) mutant in *cps-6(tm3222)* males failed to rescue the PME defect (Fig. 2F, matings 3 and 4), the nuclease activity of CPS-6 is essential for PME.

Using electron tomography, we examined how loss of *cps-6* affects PME. In *cps-6(tm3222)* zygotes, aggregates were still visible in paternal mitochondria but were smaller and fewer than in N2 zygotes, and no ghost PM were detected (Fig. 1, B, E, and G), indicating reduced and slower internal breakdown of paternal mitochondria. The autophagosome membranes started to assemble around paternal mitochondria in two- or four-cell *cps-6(tm3222)* embryos and completed enclosure by the 16-cell stage (Fig. 1, H and I), proceeding significantly slower than in N2 embryos, in which autophagosome assembly started earlier at the one-cell stage and was complete by the four-cell stage (Fig. 1, C to E). Even after autophagosome enclosure, internal breakdown of paternal mitochondria was clearly delayed (Fig. 1, I and J), because a significant portion of cristae remained superficially intact and fewer than 40% of paternal mitochondria transited into ghost PM in 16-cell

cps-6(tm3222) embryos (Fig. 1E). Some large agg PM even lingered on in 64-cell embryos (Fig. 1J), compared with 100% of paternal mitochondria either eliminated or becoming ghost PM by the four-cell N2 embryos (Fig. 1, D and E). Therefore, CPS-6 is important in mediating internal breakdown of paternal mitochondria and their enclosure by autophagosomes after fertilization.

Compromised mitochondria often show loss of membrane potential, which can be detected by tetramethylrhodamine ethyl ester (TMRE), a potential-sensitive mitochondrial dye. When N2 males prestained with TMRE and a nucleic acid dye (SYTO11)—which labeled sperm mitochondria and their mtDNA, respectively (fig. S4, A and B)—were mated with N2 hermaphrodites, paternal mitochondria were still labeled by SYTO11 in N2 zygotes, but their TMRE staining was completely lost (Fig. 3A). In comparison, staining of paternal mitochondria by potential-insensitive MTR persisted (fig. S4B). When we mated SYTO11-stained N2 males with N2 hermaphrodites in the presence of TMRE, only maternal mitochondria were stained by TMRE, and the SYTO11-positive paternal mitochondria were TMRE-negative (Fig. 3B). Therefore, paternal

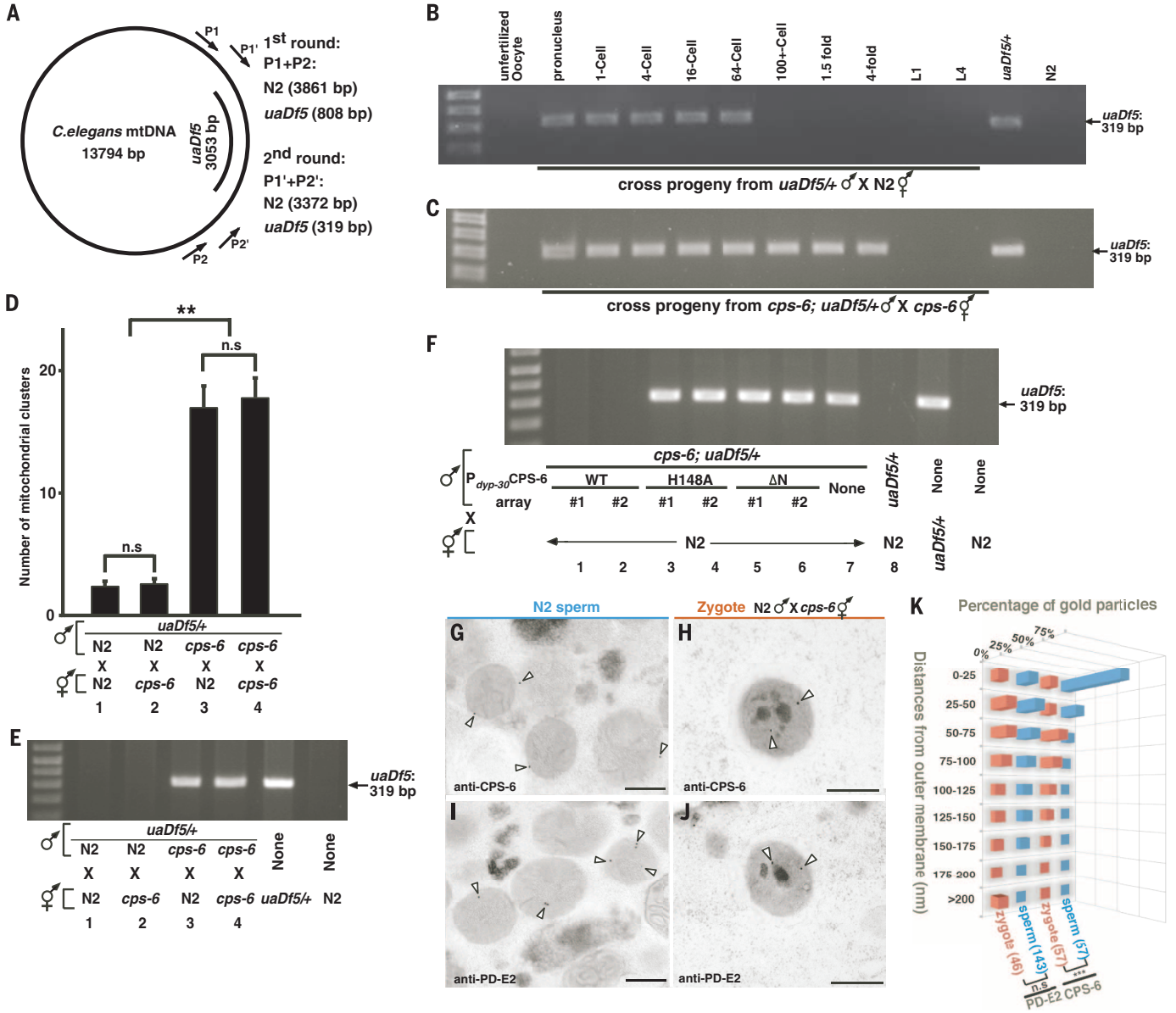

Fig. 2. CPS-6 relocates from the intermembrane space of paternal mitochondria to the matrix after fertilization to promote PME. (**A**) Diagram of *C. elegans* mtDNA, the *uaDf5* deletion, primers used in the nested PCR assays, and sizes of PCR products in N2 and *uaDf5/+* animals. (**B** and **C**) Hermaphrodites and MTR-stained males were mated as indicated. Males also carried *smIs42*, an integrated $P_{sur\text{-}5}$*sur-5::gfp* transgene used to track cross progeny (see fig. S2A). A single unfertilized oocyte and a single cross-fertilized embryo or larva (MTR- or GFP-positive) at the indicated stage was analyzed by PCR. *uaDf5/+* and N2 hermaphrodites were controls. (**D**) Quantification of MTR-stained paternal mitochondrial clusters in 64-cell embryos from the indicated crosses with MTR-stained males. Data are means ± SEM; n = 20 per cross. $^{**}P <$ 0.0001 (unpaired Student t test); n.s., not significant. (**E** and **F**) Five cross-fertilized embryos (E) or transgenic embryos (F) at approximately 100-cell stage from the indicated crosses were analyzed by PCR. (**G** to **J**) Representative immuno-EM images of mitochondria in N2 spermatozoa and paternal mitochondria in zygotes from the indicated cross. CPS-6–specific and PD-E2–specific immunogold particles are marked with arrowheads. Scale bars, 300 nm. (**K**) Histogram of the distances of 15-nm immunogold particles from the mitochondrial membrane, illustrating CPS-6's movement after fertilization. Numbers of immunogold particles scored are shown in parentheses. $^{***}P < 0.0001$ (Mann-Whitney U test). *cps-6(tm3222)* was used in all figures.

mitochondria are depolarized shortly after fertilization, preceding degradation of their mtDNA.

We used immuno-EM to determine the localization of CPS-6 in paternal mitochondria. CPS-6 immunogold particles were predominantly associated with the mitochondrial membrane in N2 spermatozoa (Fig. 2, G and K, and fig. S2G), in agreement with CPS-6's localization in mitochondrial intermembrane space. In zygotes from *cps-6(tm3222)* hermaphrodites mated with N2 males, CPS-6 immunogold particles were often located inside paternal mitochondria, away from the mitochondrial membrane (Fig. 2, H and K, and fig. S5). Because some paternal mitochondria had not been associated with autophagosomes (Fig. 2H), CPS-6 appeared to enter the matrix before the assembly of autophagosomes. The relocation of CPS-6 into the matrix after fertilization is clearly discerned when compared with the localization patterns of a mitochondrial matrix protein, the E2 subunit of pyruvate dehydrogenase (PD-E2, Fig. 2, I to K). Collectively, these different microscopy analyses provide strong evidence that paternal mitochondria are depolarized and damaged internally soon after fertilization, leading to the release of CPS-6 into the matrix to catalyze mtDNA degradation.

The autophagy and proteasome pathways promote PME in *C. elegans* (*5*–*7*). Both LGG-1, the worm LC3/Atg8 homolog necessary for autophagosome formation (*11*), and RAD-23, a ubiquitin receptor important for proteasomal degradation (*5*, *12*), act maternally to promote PME (fig. S6, A and B, and supplementary text). Analyses of the double and the triple mutants among *cps-6*, *lgg-1*, and *rad-23* indicate that *cps-6*, *lgg-1*, and *rad-23* use distinct mechanisms (mitochondrial self-destruction, autophagy, and proteasomes, respectively) to coordinate swift and efficient PME (fig. S6, C to F).

Because loss of *cps-6* slows down autophagosome formation and degradation of paternal mitochondria (Fig. 1), we further interrogated this issue by immunostaining; we found that in N2 zygotes, bright LGG-1 staining was seen clustering around MTR-stained paternal mitochondria near the site of sperm entry (fig. S4C), with 81% of paternal mitochondrial clusters colocalizing with LGG-1 autophagosomes (fig. S4E). By contrast, in *cps-6(tm3222)* zygotes, such colocalization dropped to 43% (fig. S4, D and E), indicating that loss of *cps-6* reduces autophagosome formation on paternal mitochondria. Analysis using superresolution structured illumination microscopy (SIM) revealed similar results. In N2 zygotes, the majority (77%) of paternal mitochondria were enclosed by LGG-1 autophagosomes, some (12%) were partially enclosed, and only 11% did not associate with (isolated) autophagosomes (Fig. 3, C and D, and fig. S4, F and H). By contrast, in *cps-6(tm3222)* zygotes, 51% of paternal mitochondria were isolated and only 29 and 20% of paternal mitochondria were enclosed and partially enclosed by autophagosomes, respectively (Fig. 3, E and F, and fig. S4, G and H). These findings indicate that the CPS-6 self-destruction process is important for efficient recruitment of autophagosomes to paternal mitochondria.

It has been suggested that the high rate of energy consumption during fertilization of an oocyte by many competing spermatozoa leads to increased oxidative damage and mutations in sperm mtDNA (*13*, *14*). Failure to remove paternal mitochondria with mutated mtDNA can cause incompatibility with maternal mitochondria and the nuclear genome and can adversely affect the fitness of animals (*15*–*17*). Comparison of N2 embryos with *uaDf5*/+ embryos, with four genes deleted in *uaDf5* mtDNA (*18*), revealed a factor of 23 increase in embryonic lethality from 0.4 to 9.4% (Fig. 4A, assays 1 and 3), indicating that the heteroplasmic presence of mtDNA mutations compromises embryo development. Delayed removal of *uaDf5* paternal mitochondria in embryos by loss of *cps-6* resulted in a lethality rate of 5.9%, higher by a factor of 5 to 7 than that of cross-fertilized *cps-6(tm3222)* embryos (0.7%) or that of embryos with no persistent paternal mitochondria (0.8 to 0.9%) (Fig. 4A, assays 4 to 7, and supplementary text). Moreover, delayed clearance of *uaDf5* paternal mitochondria slowed cell divisions, an energy-driven process, during *C. elegans* embryogenesis, because the average durations of cell divisions in two different cell lineages (MS and P) were significantly prolonged in *uaDf5*/+ embryos and by delayed removal of *uaDf5* paternal mitochondria (Fig. 4, B and C, fig. S7, and supplementary

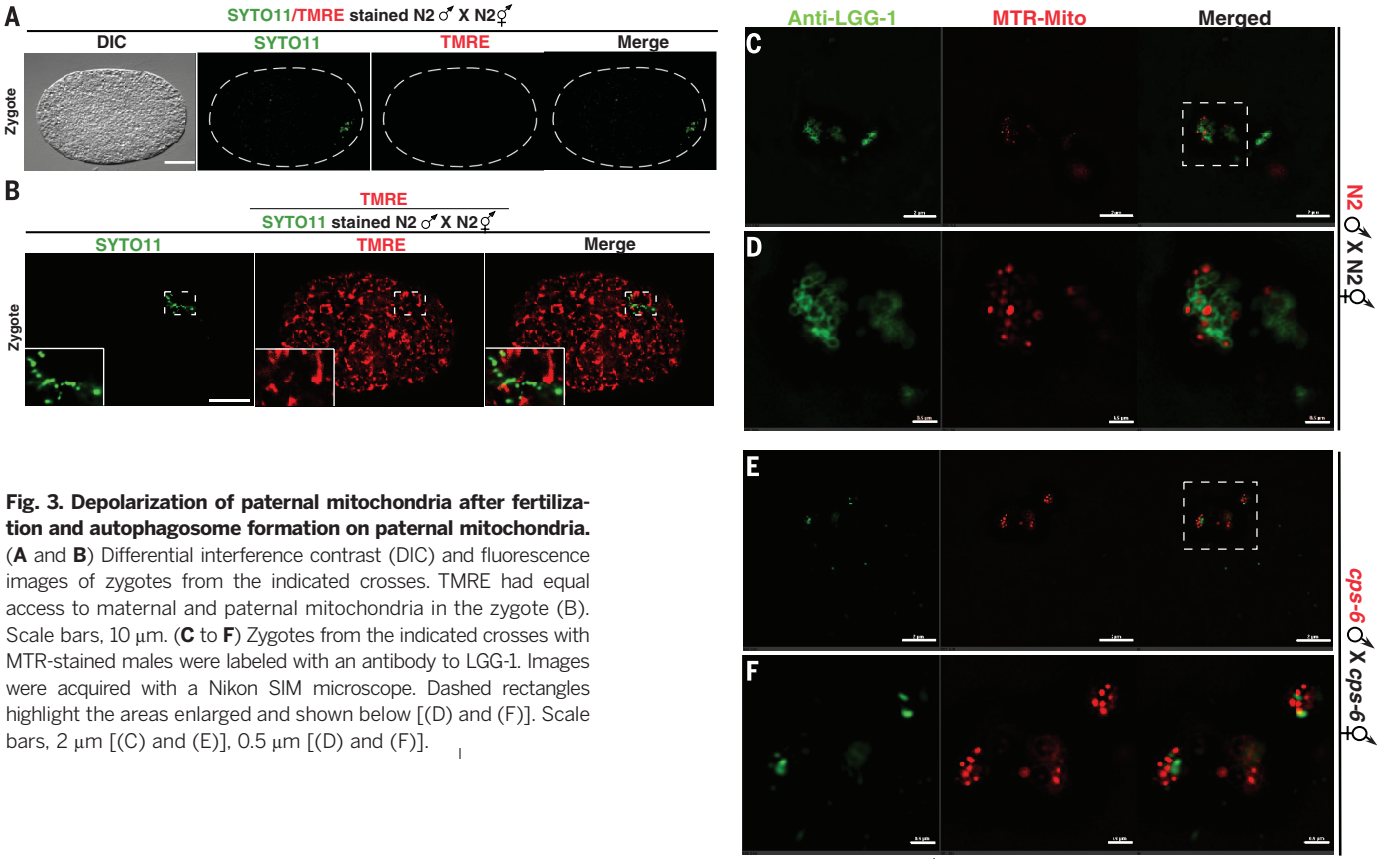

Fig. 3. Depolarization of paternal mitochondria after fertilization and autophagosome formation on paternal mitochondria. (**A** and **B**) Differential interference contrast (DIC) and fluorescence images of zygotes from the indicated crosses. TMRE had equal access to maternal and paternal mitochondria in the zygote (B). Scale bars, 10 μm. (**C** to **F**) Zygotes from the indicated crosses with MTR-stained males were labeled with an antibody to LGG-1. Images were acquired with a Nikon SIM microscope. Dashed rectangles highlight the areas enlarged and shown below [(D) and (F)]. Scale bars, 2 μm [(C) and (E)], 0.5 μm [(D) and (F)].

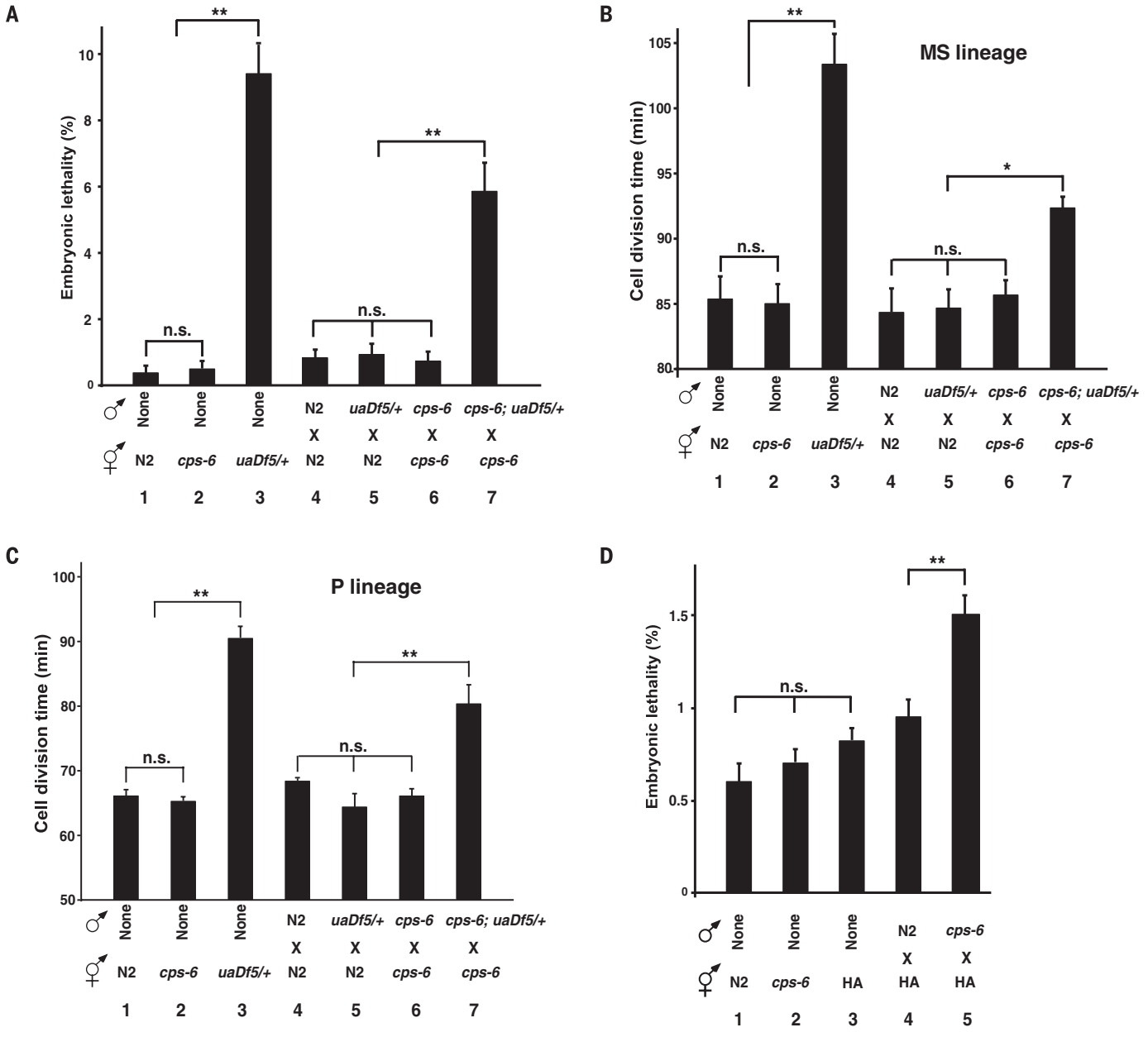

Fig. 4. Delayed removal of paternal mitochondria increases embryonic lethality and cell division durations. (**A** to **D**) The embryonic lethality rate [(A) and (D)] and durations of cell divisions in the MS lineage (B) and P lineage (C) were scored in self-fertilized embryos (1 to 3) or cross-fertilized embryos from crosses (4 to 7) of the indicated genotypes. All males carried *smIs42* and were stained with MTR to assist identification of zygotes [(B) and (C)]. Data are means ± SEM; $n > 1000$ embryos per cross at 25°C [(A) and (D)] and $n = 3$ embryos per cross at 20°C [(B) and (C)]. *$P < 0.05$, **$P < 0.001$ (unpaired Student t test).

text). These results provide evidence that delayed clearance of mutated paternal mitochondria leads to decreased fitness at the cellular and organismal levels and presents an evolutionary disadvantage.

Next, we examined the consequence of delayed removal of wild-type paternal mitochondria by mating two different *C. elegans* wild-type strains, the Bristol strain (N2) and the Hawaii strain (HA). Delayed removal of wild-type Bristol paternal mitochondria in HA embryos due to loss of paternal *cps-6* also resulted in a significantly higher percentage of embryonic lethality than that seen in HA embryos without persistent paternal mitochondria (Fig. 4D, assays 4 and 5, and fig. S6G, matings 2 and 4; see also supplementary text). Therefore, delayed clearance of wild-type paternal mitochondria slightly different from maternal mitochondria also compromises animal development, which suggests that transmission of paternal mitochondria among different wild-type variants is evolutionarily disadvantageous.

Our results show that soon after fertilization, paternal mitochondria are depolarized and lose their inner membrane integrity, which apparently marks them for degradation by autophagy (*19*, *20*). The inner membrane breakdown probably triggers the entry of the intermembrane CPS-6 into the matrix of paternal mitochondria to degrade mtDNA, which encodes 12 mitochondrial proteins, two rRNAs, and 22 tRNAs that are essential for normal functions and maintenance of mitochondria (*1*, *13*, *18*). Degradation of mtDNA is detrimental, which accelerates breakdown of paternal mitochondria and could promote externalization of signals recognized by the autophagy or proteasome machinery (*19*, *20*), leading to PME (fig. S8). Consistent with this model, loss of paternal *cps-6* delays internal breakdown of paternal mitochondria and their enclosure and degradation by the autophagy

machinery. Interestingly, delayed removal of either mutant or slightly different wild-type paternal mitochondria results in increased embryonic lethality in heteroplasmic animals, likely due to incompatibility in cellular signaling between the mitochondrial and nuclear genomes (*15*, *17*). This provides evidence that persistence of paternal mitochondria compromises animal development and may be the impetus for maternal inheritance of mitochondria. DeLuca and O'Farrell showed that endonuclease G mediated the degradation of sperm mitochondrial DNA during *Drosophila* spermatogenesis before fertilization and hypothesized that this degradation helped prevent paternal mtDNA transmission (*21*). In contrast, we find in *C. elegans* that CPS-6 acts after fertilization to mediate degradation of both paternal mitochondria and mtDNA to facilitate their autophagic degradation. These findings imply a conserved role of endonuclease G in paternal mtDNA elimination and expand the roles of this nuclease beyond apoptosis and mitochondrial maintenance (*8*, *9*, *22*).

REFERENCES AND NOTES

1. S. E. Calvo, V. K. Mootha, *Annu. Rev. Genomics Hum. Genet.* **11**, 25–44 (2010).
2. X. Wang, *Genes Dev.* **15**, 2922–2933 (2001).
3. M. Sato, K. Sato, *Biochim. Biophys. Acta* **1833**, 1979–1984 (2013).
4. B. Levine, Z. Elazar, *Science* **334**, 1069–1070 (2011).
5. Q. Zhou, H. Li, D. Xue, *Cell Res.* **21**, 1662–1669 (2011).
6. S. Al Rawi *et al.*, *Science* **334**, 1144–1147 (2011).
7. M. Sato, K. Sato, *Science* **334**, 1141–1144 (2011).
8. J. Parrish *et al.*, *Nature* **412**, 90–94 (2001).
9. L. Y. Li, X. Luo, X. Wang, *Nature* **412**, 95–99 (2001).
10. J. L. Lin *et al.*, *J. Biol. Chem.* **287**, 7110–7120 (2012).
11. K. Jia, B. Levine, *Adv. Exp. Med. Biol.* **694**, 47–60 (2010).
12. K. Madura, *Trends Biochem. Sci.* **29**, 637–640 (2004).
13. D. C. Wallace, *Environ. Mol. Mutagen.* **51**, 440–450 (2010).
14. J. M. Cummins, *Hum. Reprod.* **15** (suppl. 2), 92–101 (2000).
15. M. S. Sharpley *et al.*, *Cell* **151**, 333–343 (2012).
16. M. Schwartz, J. Vissing, *N. Engl. J. Med.* **347**, 576–580 (2002).
17. N. Lane, *BioEssays* **33**, 860–869 (2011).
18. W. Y. Tsang, B. D. Lemire, *Biochem. Cell Biol.* **80**, 645–654 (2002).
19. G. Ashrafi, T. L. Schwarz, *Cell Death Differ.* **20**, 31–42 (2013).
20. K. Wang, D. J. Klionsky, *Autophagy* **7**, 297–300 (2011).
21. S. Z. DeLuca, P. H. O'Farrell, *Dev. Cell* **22**, 660–668 (2012).
22. C. McDermott-Roe *et al.*, *Nature* **478**, 114–118 (2011).

ACKNOWLEDGMENTS

We thank T. Blumenthal, R. Poyton, and K. Krauter for comments and H. Zhang for strains and antibodies. Supported by March of Dimes grant 1-FY14-300 and NIH grants GM59083, GM79097, and GM118188 (D.X.) and Research Grants Council of Hong Kong grant AoE/M-05/12 (B.-H.K.).

SUPPLEMENTARY MATERIALS

www.sciencemag.org/content/353/6297/394/suppl/DC1
Materials and Methods
Supplementary Text
Figs. S1 to S8
Table S1
Movie S1
References (*23*–*37*)

14 February 2016; accepted 15 June 2016
Published online 23 June 2016
10.1126/science.aaf4777

CANCER IMMUNOTHERAPY

Cdk5 disruption attenuates tumor PD-L1 expression and promotes antitumor immunity

R. Dixon Dorand,[1,2] Joseph Nthale,[2,3] Jay T. Myers,[2,3] Deborah S. Barkauskas,[2,3] Stefanie Avril,[1,4] Steven M. Chirieleison,[1] Tej K. Pareek,[2,3] Derek W. Abbott,[1,4] Duncan S. Stearns,[2,3,4] John J. Letterio,[2,3,4] Alex Y. Huang,[1,2,3,4]*† Agne Petrosiute[2,3,4]*†

Cancers often evade immune surveillance by adopting peripheral tissue–tolerance mechanisms, such as the expression of programmed cell death ligand 1 (PD-L1), the inhibition of which results in potent antitumor immunity. Here, we show that cyclin-dependent kinase 5 (Cdk5), a serine-threonine kinase that is highly active in postmitotic neurons and in many cancers, allows medulloblastoma (MB) to evade immune elimination. Interferon-γ (IFN-γ)–induced PD-L1 up-regulation on MB requires Cdk5, and disruption of Cdk5 expression in a mouse model of MB results in potent $CD4^+$ T cell–mediated tumor rejection. Loss of Cdk5 results in persistent expression of the PD-L1 transcriptional repressors, the interferon regulatory factors IRF2 and IRF2BP2, which likely leads to reduced PD-L1 expression on tumors. Our finding highlights a central role for Cdk5 in immune checkpoint regulation by tumor cells.

Cyclin-dependent kinase 5 (Cdk5) is a nonstereotypical Cdk whose activity depends on coactivators, p35 and/or p39. A proline-directed serine-threonine kinase (*1*), Cdk5 is essential in central nervous system (CNS) development (*2*, *3*). Cdk5 also contributes to angiogenesis, apoptosis, myogenesis, vesicular transport, and senescence in nonneuronal cells, including tumors (*4*–*6*), which makes Cdk5 a potential therapeutic target in cancers (*7*–*9*). We explored whether Cdk5 plays a role in medulloblastoma (MB), a common malignant pediatric CNS tumor.

MB cell lines and clinical specimens expressed Cdk5, p35, and p39 (Fig. 1A and fig. S1A). Cdk5-specific kinase activity could be abolished in vitro by roscovitine, a nonselective inhibitor against Cdks 1, 2, 5, 7, and 9 (fig. S1B) (*10*). To interrogate Cdk5-specific functions, we disrupted Cdk5 in wild-type murine MB cells (MM1 WT) by short hairpin–mediated RNA interference (MM1 shCdk5) and clustered regularly interspaced short palindromic repeats (CRISPR)–Cas9–targeted mutation (MM1 crCdk5), with nontargeting constructs as controls (MM1 shNS and MM1 crNeg). A reduction in Cdk5 was confirmed at the transcript (fig. S1C) and protein levels (fig. S1D). In vitro, there were no significant differences in cell proliferation among all constructs (fig. S1, E and F) (*1*).

[1]Department of Pathology, Case Western Reserve University School of Medicine, Cleveland, OH 44106, USA. [2]Division of Pediatric Hematology-Oncology, Department of Pediatrics, Case Western Reserve University School of Medicine, Cleveland, OH 44106, USA. [3]Angie Fowler Adolescent and Young Adult Cancer Institute and University Hospitals Rainbow Babies and Children's Hospital, Cleveland, OH 44106, USA. [4]Case Comprehensive Cancer Center, Case Western Reserve University School of Medicine, Cleveland, OH 44106, USA.
*These authors contributed equally to this work. **†Corresponding author. Email: ayh3@case.edu (A.Y.H.); axp125@case.edu (A.P.)**

To assess MB growth in vivo, 5×10^4 Cdk5-deficient or control cells were inoculated subcutaneously (s.c.) into the flanks of immunodeficient mice. All mice developed comparable-sized tumors by day 14 (fig. S2, A to C). However, 78 to 50% of C57BL/6 mice injected s.c. with Cdk5-deficient MB cells showed tumor-free survival (TFS) at 19 and 42 days, whereas mice injected with WT and control tumors exhibited 0 and 7% TFS after 19 days, respectively (Fig. 1B and fig. S3A). Mice injected with Cdk5-deficient MB cells developed significantly smaller tumors (0.02 ± 0.04 g) than mice injected with WT (0.91 ± 0.39 g) or NS (0.51 ± 0.21 g) cells (fig. S3B). These data suggest a T cell–dependent rejection mechanism of Cdk5-deficient MM1 cells. This interpretation is supported by the observation that Cdk5 expression inversely correlated with T cell infiltration in human MB (Fig. 1C and fig. S2D).

To identify T cell populations mediating this potent rejection, we depleted $CD8^+$ T cells, $CD4^+$ T cells, or both subsets in mice inoculated with MM1 crCdk5 or crNeg cells (5×10^4 s.c.). By day 11, 100% of mice injected with MM1 crNeg and 80% of mice receiving MM1 crCdk5 developed measurable tumors (Fig. 1B), although MM1 crNeg tumors were 8 times the size of MM1 crCdk5 tumors (808.8 ± 382.1 versus 101.1 ± 92.9 mm^3) (Fig. 1D). Depletion with CD4-specific (αCD4) antibody alone or with both αCD4 and αCD8 antibodies resulted in 100% MM1 crCdk5 tumor incidence accompanied by rapid tumor growth, whereas CD8 depletion alone yielded 30% TFS, similar to isotype control (Fig. 1D). Among mice receiving isotype antibody, three of eight crCdk5 tumor outgrowths regressed starting on day 17, whereas three of nine crCdk5 tumor outgrowths among mice depleted of $CD8^+$ T cells regressed starting on day 25; these outgrowths contributed

Editor's Summary

Eliminating paternal mitochondria

During fertilization, the oocyte and sperm each bring their mitochondria to the union. Shortly afterward, the paternal mitochondria are degraded, and only the maternal mitochondria are conveyed to the progeny. Zhou *et al.* observed that the integrity of the inner membrane of paternal mitochondria is compromised, which apparently marks them for degradation (see the Perspective by van der Bliek). Autophagy commences by mitochondrial endonuclease G relocating from the intermembrane space into the matrix and subsequently degrading the paternal mitochondrial DNA. Any delay in this process increases embryonic lethality.

Science, this issue p. 394; see also p. 351